


## Pump-laser-wavelength dependence of population inversion in $N_2^+$

Liang Xu <sup>1,\*</sup>, Chaohui Zhou,<sup>1</sup> Guangyu Fan,<sup>1</sup> Hongyang Cheng,<sup>1</sup> Aurélien Houard <sup>2</sup>, André Mysyrowicz,<sup>2</sup> Vladimir T. Tikhonchuk <sup>3,4</sup> and Yi Liu<sup>1,5,†</sup>

<sup>1</sup>Shanghai Key Lab of Modern Optical System, University of Shanghai for Science and Technology, 516, Jungong Road, 200093 Shanghai, People's Republic of China

<sup>2</sup>Laboratoire d'Optique Appliquée, ENSTA Paris, CNRS, Ecole Polytechnique, Institut Polytechnique de Paris, 91762 Palaiseau, France

<sup>3</sup>University of Bordeaux-CNRS-CEA, CELIA, UMR 5107, 33405 Talence, France

<sup>4</sup>Extreme Light Infrastructure ERIC, ELI-Beamlines Facility, Za Radnicic 835, 25241 Dolní Břežany, Czech Republic

<sup>5</sup>CAS Center for Excellence in Ultra-intense Laser Science, Shanghai 201800, China



(Received 26 September 2023; accepted 1 December 2023; published 24 January 2024)

We investigate the pump wavelength dependence of population inversion in a nitrogen ion when nitrogen gas is irradiated by a femtosecond laser pulse in the wavelength range from ultraviolet to near-infrared. It is found that the population inversions corresponding to the transitions at 391 and 428 nm are very sensitive to the laser wavelength, with extreme values near 400 and 1000 nm. For the ultraviolet pump, the population inversions for 391 and 428 nm transitions occur at different wavelengths: a maximum inversion for the first corresponds to a minimum for the second. This is attributed to the near-resonance single-photon transition combined with the Raman process. A significantly stronger inversion is observed for the near-infrared laser, with the maximum depending on the laser intensity, ascribed to the ac Stark effect. The Floquet theory confirms this conclusion and reveals that the three-photon transition assisted by the strong laser field leads to this enhanced population inversion. This study provides the optimal conditions for air lasing based on ionic transitions of nitrogen molecules.

DOI: [10.1103/PhysRevA.109.013518](https://doi.org/10.1103/PhysRevA.109.013518)

### I. INTRODUCTION

With intense ultrashort laser pulses, it is possible to achieve remote optical amplification from the major constituents of air: nitrogen and oxygen. The cavity-free optical amplification in air was reported in 2011 [1,2] and has attracted much attention due to its potential application in standoff spectroscopy [3,4], sensing [5,6], and advanced light sources [7,8]. Forward and backward amplification has been observed in atomic oxygen and nitrogen, molecular nitrogen, and singly ionized molecular nitrogen [9]. In contrast to cavity-free lasing in atoms and neutral molecules for which a good physical explanation is provided, the case of nitrogen ion  $N_2^+$  is still controversial. Two theoretical models have been proposed to explain the strong amplification observed at 391 and 428 nm. The first model accounts for population inversions corresponding to the transitions between the initial state  $B^2\Sigma_u^+$  (designated as  $B$ ) with vibrational level  $v = 0$  and final states  $X^2\Sigma_g^+$  (denoted as  $X$ ) with  $v = 0$  and 1, which is predicted by the three-state coupling model [10–12]. The second model considers a simultaneous two-photon emission or absorption process between  $B0$  and intermediate level  $A^2\Pi_u$  (denoted as  $A$ ) transiting via  $X0$  and  $X1$  [13,14]. Amplification of the optical field in the plasma channel is the key element of this model. Kleine *et al.* used high-harmonic spectroscopy to track the strong field ionization and fragmentation dynamics

of  $N_2^+$  upon interaction with an ultrashort 800-nm laser pulse [15]. Recently, Danylo *et al.* measured the evolution of ionic population in  $N_2^+$  [16]. Both their observations support the second model. In addition, a rotational quantum beat can suppress absorption while leaving the stimulated emission intact transiently, leading to lasing without inversion [17].

Though the role of population inversion responsible for air lasing has not been fully determined yet, there is no doubt that population inversion is an important factor in favoring strong amplification of the seed pulse. Xu *et al.* predicted an increased population inversion by increasing the 800-nm laser pulse duration [10]. The polarization-modulated ultrashort laser pulse solely or combined with the middle-infrared laser may result in a giant enhancement of  $N_2^+$  lasing [18,19]. Zhang *et al.* studied the dependence of population  $B$  and  $X$  as a function of the pump laser wavelength [12]. However, their calculation assumed a molecular alignment with respect to the laser polarization and only discussed the 391-nm case with a range of the pump laser wavelengths from near-infrared to middle-infrared.

In this paper, we theoretically investigate the population distribution of levels  $B0$ ,  $X0$ , and  $X1$  responsible for the lasing transitions at 391 and 428 nm as a function of pump wavelength with a broad range from ultraviolet to near-infrared and different laser intensities. We find an anticorrelation between the population inversions for 391- and 428-nm transitions in the ultraviolet region. The origin of this effect is identified by analyzing the temporal evolution of the populations during the pump pulse duration. More significant enhancements of population inversions for the 391- and 428-nm transitions

\*liangxu2021@usst.edu.cn

†yi.liu@usst.edu.cn

are found for the laser wavelengths 900–1050 nm. This phenomenon is explained by the dominance of the three-photon transition in the strong laser field with intensity-dependent resonance due to the ac Stark shift. The results of numerical simulations are confirmed with the theoretical analysis using the Floquet approach. The paper is organized as follows. The theoretical background and the numerical method are introduced in Sec. II. Simulation results are discussed in Sec. III and conclusions are presented in Sec. IV. Hartree atomic units are used throughout the paper unless stated otherwise.

## II. THEORETICAL BACKGROUND

Two theoretical models, the density matrix and the time-dependent Schrödinger equation, are extensively used for describing a coherent light-molecule interaction system [20]. While the results of these two approaches are equivalent, the first is better suited for a multiple-electron system when considering simultaneously ionization and excitation, and is numerically more efficient. We adopt the density matrix framework here. The dynamics of  $N_2$  ionization and  $N_2^+$  excitation driven by an intense laser pulse is described by the Bloch equation [12,14,21]

$$\frac{d\rho}{dt} = -i[H, \rho] + W. \quad (1)$$

Here  $\rho$ ,  $H$ , and  $W$  represent the density matrix, system Hamiltonian, and instantaneous ionization rate, respectively. The first term on the right-hand side is the Poisson bracket, which describes the transitions between vibronic levels in  $N_2^+$  molecule. The Hamiltonian  $H$  consists of diagonal elements  $\varepsilon_{\nu\nu}$  and off-diagonal elements  $H_{\nu\nu'}$ , which correspond to the energies of vibrational eigenstates and the interaction between the laser field and the molecule, respectively. In addition to the ground state  $X$ , two electronic excited states are considered. The transition between  $X$  and  $A$  states,  $H_{XA}^{\nu\nu'} = -\mu_{XA}^{\nu\nu'} E(t) \sin \theta$ , is favored for the angle  $\theta$  between the molecule axis and the direction of laser electric field  $E$  close to  $90^\circ$  (perpendicular orientation). The transition between  $X$  and  $B$  states,  $H_{XB}^{\nu\nu'} = -\mu_{XB}^{\nu\nu'} E(t) \cos \theta$  is favored for the parallel orientation. Other electronic excited states are neglected because of their large transition energy. In total, as shown in Fig. 1, 13 vibrational levels are considered, that is,  $X$  ( $\nu = 0-2$ ),  $A$  ( $\nu = 0-4$ ), and  $B$  ( $\nu = 0-4$ ). The transition dipole moments  $\mu_{XA}^{\nu\nu'}$  and  $\mu_{XB}^{\nu\nu'}$  and the corresponding energies are listed in Table I of Appendix A.

The instantaneous ionization rate  $W$  is represented as

$$W_{MM'}^{\nu\nu'}(\theta, t) = C_M^{v*}(\theta, t) C_{M'}^{\nu'}(\theta, t), \quad (2)$$

where index  $M$  denotes the  $X$ ,  $A$ , or  $B$  electronic state and index  $\nu$  denotes the vibrational quantum number. The diagonal elements of  $W$  denote the instantaneous ionization rate, which is calculated by the molecular Ammosov-Delone-Krainov theory [22–24]. The off-diagonal ones describe the coherence of ionization injection. Here we assume that the free electrons from different electronic states have the same momenta. Then the off-diagonal elements take real positive values with the coefficient  $C_M^{\nu}$  defined by a square root of the product of ionization rate, the corresponding Franck-Condon factor, and the remaining population of neutral

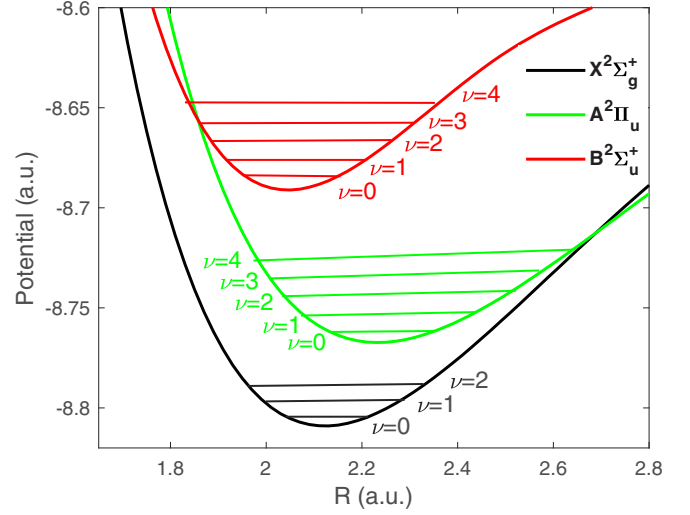


FIG. 1. Energy diagram in  $N_2^+$ : the relevant potential energy curves for three electronic states  $X^2\Sigma_g^+$  (black),  $A^2\Pi_u$  (green), and  $B^2\Sigma_u^+$  (red) as well as the corresponding nuclear vibrational states labeled by the quantum number  $\nu$ .

molecules  $N_2$ . The linearly polarized laser field is expressed by

$$E(t) = E_0 \cos(\omega t) \sin^2(\pi t/\tau), \quad (3)$$

where  $E_0$ ,  $\omega$ , and  $\tau$  represent the laser amplitude, angular frequency, and pulse duration. The results below are presented for a typical value  $\tau = 60$  fs, though similar results are obtained for the pulse duration from 40 fs to 80 fs. The laser wavelength  $\lambda = 2\pi c/\omega$  is varied in the range from 300 nm to 1200 nm and laser intensities of 1, 2, and  $3 \times 10^{14}$  W/cm<sup>2</sup> are considered.

Equation (1) is solved numerically by using the fixed-step fourth-order Runge-Kutta technique with the time step  $dt = 0.02$  a.u. and the initial condition  $\rho(\theta, t = 0) = 0$ . The simulations are performed for the entire pulse duration  $[0, \tau]$  for different angles  $\theta = 0, \pi/36, \dots, \pi$ . Symmetry in the plane perpendicular to the laser polarization is assumed. The final population distribution is obtained via averaging over the polar angle

$$\bar{P}_M^{\nu} = \frac{\int_0^\pi \rho_{MM}^{\nu\nu}(\theta, t_{\text{end}}) \sin \theta d\theta}{\int_0^\pi \sin \theta d\theta}. \quad (4)$$

Population inversions for 391- and 428-nm lasing are calculated as  $P_{391} = \bar{P}_B^0 - \bar{P}_X^0$  and  $P_{428} = \bar{P}_B^0 - \bar{P}_X^1$ , respectively. Convergence of the calculations was tested using more vibrational levels, finer angular resolution, and smaller time steps, whereas almost identical results were obtained.

## III. RESULTS AND DISCUSSION

Figure 2 shows the dependence of the population inversions  $P_{391}$  and  $P_{428}$  on the laser wavelength for three typical laser intensities for filaments in air. Positive population inversions corresponding to the 428-nm transition (dashed lines) are observed for all wavelengths and intensities. This is explained by the fact that level  $X1$  is scarcely populated:

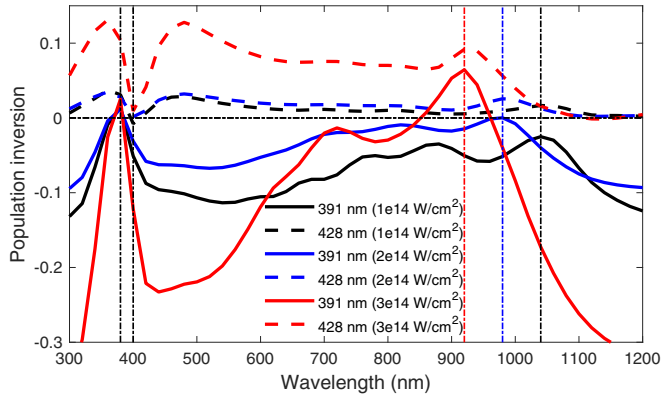


FIG. 2. Dependence of the population inversion on the laser wavelength. Solid lines show the population inversion between  $B0$  and  $X0$  levels corresponding to the transition at 391 nm. Dashed lines show the inversion between  $B0$  and  $X1$  levels corresponding to the transition at 428 nm. Black, blue, and red lines correspond to the laser peak intensity 1, 2, and  $3 \times 10^{14}$  W/cm<sup>2</sup>. The results for  $1 \times 10^{14}$  W/cm<sup>2</sup> (black lines) are multiplied by a factor of 100.

Direct ionization to this level is suppressed due to the small Franck-Condon factor and transition from the  $X0$  level is forbidden because of the homonuclear diatomic molecule  $N_2^+$ . By contrast, the population inversion for emission at 391 nm (solid lines) strongly depends on the laser wavelength, showing no population inversion in the range from 400 nm to 700 nm and maximums in the near-infrared and ultraviolet 380 nm regions. Specifically, in the near-infrared band, as the laser intensity increases from 1 to  $3 \times 10^{14}$  W/cm<sup>2</sup>, the wavelength for maximum population inversion appears around 1040 nm and shifts to 920 nm. The vertical dash-dotted lines mark the positions of maximums.

As shown in Fig. 2, the population inversion for 391-nm emission is already created at the laser intensity  $2 \times 10^{14}$  W/cm<sup>2</sup> (black solid line). This intensity value is smaller than that shown in previous reports [2,10,11,24,25], though the ionization probability is low at this intensity. The wavelengths for maximum population inversion for 391- and 428-nm transitions occur at the same wavelength in the infrared region. As shown below, this can be ascribed to the population increase in level  $B0$  since this level is common for both transitions. By contrast, there is an anticorrelation of population inversions in the ultraviolet region. The minimum at about 400 nm for the emission at 428 nm coincides nearly with the maximum for the emission at 391 nm. This is indicated by the two left vertical dash-dotted lines in Fig. 2. These observations highlight the significant difference in the excitation dynamics between the infrared and ultraviolet domains.

To better understand the mechanism of population inversion in the ultraviolet region, we consider the evolution of relevant populations at the typical intensity  $2 \times 10^{14}$  W/cm<sup>2</sup>. The coupling between  $X$  and  $A$  states is very weak in this range because of a large detuning between photon energy and the energy of transition. Nevertheless, the direct ionization for molecules aligned in the plane perpendicular to the laser polarization,  $\theta = 90^\circ$ , should not be ignored. Hence, we select

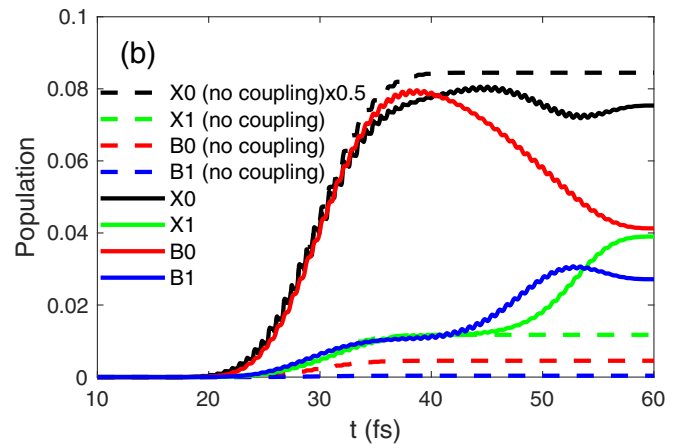
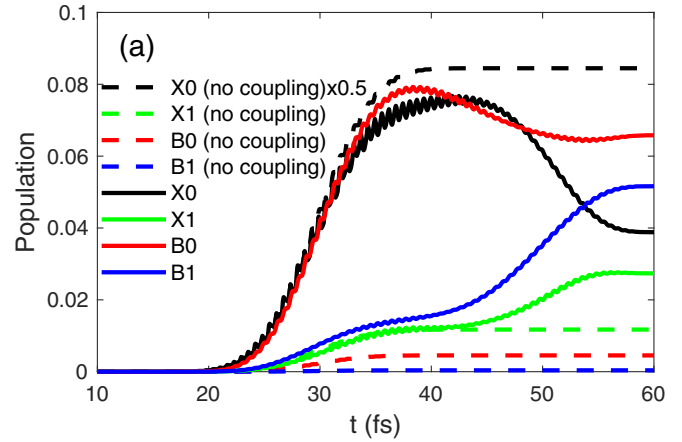


FIG. 3. The time dependence of populations in levels  $X0$  (black),  $X1$  (green),  $B0$  (red), and  $B1$  (blue) for  $\theta = 45^\circ$ . Laser peak intensity is  $2 \times 10^{14}$  W/cm<sup>2</sup>; the wavelength is (a) 380 nm and (b) 400 nm. The dashed lines show the calculation where only ionization is included. The result for  $X0$  (black dashed line) is multiplied by a factor of 0.5.

an intermediate angle  $\theta = 45^\circ$  and trace the time dependence of populations in levels  $X$  and  $B$  for two laser wavelengths of 380 nm and 400 nm, as shown in Fig. 3.

The results considering only ionization processes are also shown for comparison with dashed lines. The dominant process is the ionization of neutral molecules to the ground level  $X0$  in  $N_2^+$ , while excitation to the levels  $B0$  and  $B1$  is due to the single-photon transitions. A notable fraction of ions in Figs. 3(a) and 3(b) are quickly transferred to the  $B0$  level before 40 fs. However, as shown in Fig. 3(a), level  $B1$  is populated directly from  $X0$  in the second half of the pulse and partially decays into  $X1$  via the Stokes Raman process. Conversely, for the laser wavelength at 400 nm shown in Fig. 3(b), the population of level  $B0$  is partially transferred to  $X1$  and then returns to  $B1$  via the anti-Stokes Raman effect, which is favored by the resonance interaction of the  $X1$ - $B1$  transition channel with a 400-nm photon. These coherent processes maximize the population in level  $X1$  and minimize that in  $B0$ . They are at the origin of the minimum population inversion for 428-nm emission for the laser wavelength of about 400 nm. To summarize briefly, the near-resonance

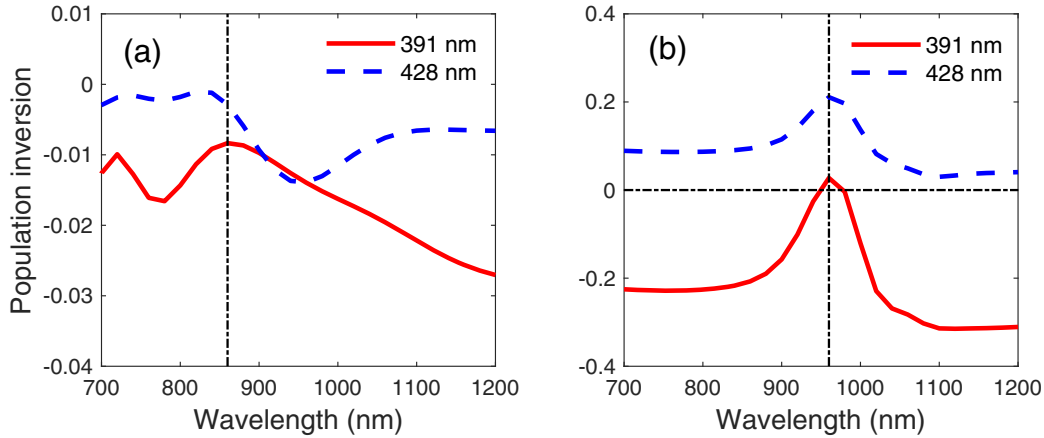


FIG. 4. Dependence of population inversion for the transitions at 391 nm (red solid lines) and 428 nm (blue dashed lines) on the laser wavelength for the molecule alignment angle (a)  $\theta = 90^\circ$  and (b)  $\theta = 0^\circ$ . Laser intensity is  $I = 2 \times 10^{14}$  W/cm<sup>2</sup>.

single-photon transmission combined with the Raman process are responsible for the peak of 391-nm inversion at 380 nm and the dip of 428-nm inversion at 400 nm. We notice that a similar mechanism of population inversion was discussed in Ref. [26].

In contrast to the ultraviolet case, the enhanced peaks of population inversion in the near-infrared range show an intensity dependence, which suggests an importance of the intensity-modulated ac Stark effect. To reveal the underlying mechanism, we consider separately two representative molecular alignments, as demonstrated in Fig. 4. In the case of transverse orientation shown in Fig. 4(a), ionization to the  $B$  level dominates and the population in  $B0$  is very small because of its larger ionization energy. Although a fraction of molecules is transferred from  $X0$  to the vibrational levels  $\nu = 0, 1, 2$  in  $A$ , this single-photon transition is insufficient to create inversions for 391-nm and 428-nm emissions. As shown in Fig. 4(b), the situation is quite different for the molecules aligned parallel to the laser field. Although the transition from the  $X0$  to  $A$  state is suppressed, molecules are transferred efficiently from the  $X0$  to  $B0$  level, thus creating population inversions. This process of the direct  $X0$ - $B0$  transition is different from the transfer through the intermediate  $A$  state studied in Refs. [10,11,14,25,27].

The direct transfer  $X0$ - $B0$  in the case of parallel orientation of a molecule, shown in Fig. 4(b), is a three-photon process. Indeed, according to the transition rules, only odd-photon processes between  $X$  and  $B$  states are allowed. The field-free energy gap between  $X0$  and  $B0$  levels is 0.1175 a.u. (3.2 eV), and the single-, three-, and five-photon transitions correspond to the laser wavelengths 391 nm, 1173 nm, and 1955 nm. The single-photon transition is already considered: it corresponds to the ultraviolet region. The three-photon resonant wavelength of 1173 nm is quite different from the maximum population inversion observed at the laser wavelength of 980 nm. The ac Stark effect can explain this blue shift of the three-photon resonance phenomenologically.

Molecules in a strong laser field are exposed to the ac Stark effect. While it is accounted for in the density matrix formalism Eq. (1), it would be interesting to evaluate it

qualitatively. The Stark shift can be estimated theoretically using the Floquet theory [28], which considers the interaction of a quantum system with an external ac field at the main frequency and its harmonics. The structure of the Floquet matrix is shown in Appendix B. It contains diagonal terms describing quantum levels and nonzero off-diagonal terms accounting for the coupling to the external field and its harmonics. The laser-dressed eigenstates are obtained by diagonalizing the Floquet matrix. We consider a laser field with a constant amplitude and account for the transitions including up to five photons.

The dependence of energy shift of  $X0$  and  $B0$  levels on laser intensity is presented in Fig. 5 for the representative laser wavelengths of 900 and 1200 nm. Similarly to the case of the dc Stark effect, the ground level shifts downward and the excited level moves upward; that is, the gap increases with the laser intensity. The three-photon interaction makes the dominant contribution. In the case of a laser wavelength of 900 nm shown in Fig. 5(a), the energy of three photons is larger than the free-field energy gap. Therefore, the transition approaches the resonance as the laser intensity increases. By contrast, in the case of 1200 nm, the energy of three photons is smaller than the free-field gap. Therefore, as the laser intensity rises, the mismatch increases and the system moves out of resonance more and more, as presented in Fig. 5(b).

Calculations performed for other laser wavelengths from 900 nm to 1200 nm confirm that the energy gap always increases with the laser intensity for the three-photon process. This is consistent with a monotonous blue shift of the wavelength for maximum population inversion with intensity shown in Fig. 2. This analysis confirms that among two competing channels of population inversion: the parallel three-photon transition between  $X0$  and  $B0$  levels and the perpendicular single-photon two-step transition through the  $A$  states, the first channel dominates. As a matter of fact, the dynamic three-photon process is very complicated in interwoven time and frequency domains, where the interactions between all vibrational states via light fields contribute to the multiphoton transition together. Thus, the Floquet theory can only give a rough picture here.



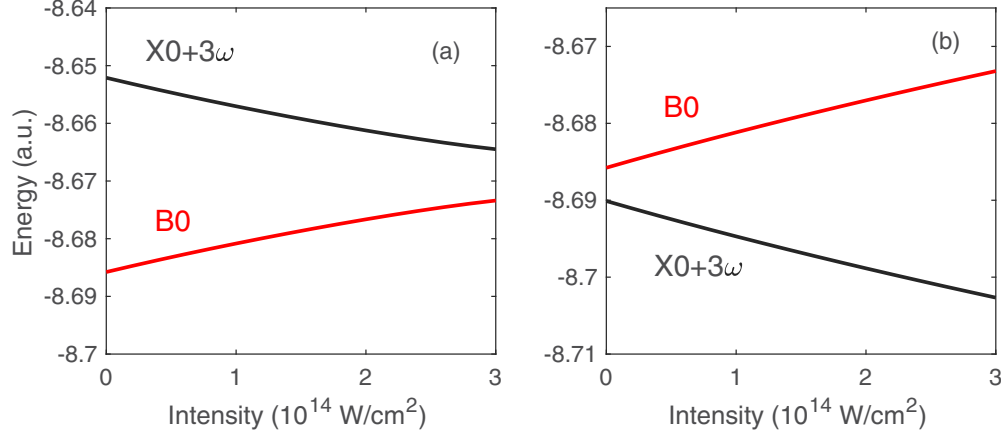


FIG. 5. Dependence of the shifts of  $X0$  and  $B0$  energy levels on the laser intensity for the laser wavelength (a) 900 nm and (b) 1200 nm. Up to five-photon transitions are considered in the Floquet matrix.

#### IV. CONCLUSION

We studied the dependence of  $N_2$  molecule ionization and ion  $N_2^+$  excitation on the wavelength and intensity of a femtosecond laser pulse. The density matrix equations based on the coherent ionization-coupling model are solved numerically, assuming an isotropic orientation of the molecules with respect to the laser polarization. The combined effect of ionization and excitation results in the population inversion between  $B0$  and  $X0$  and  $X1$  states in two particular spectral domains of near 400 and 1000 nm, corresponding to the resonance single-photon and three-photon transitions between the ground state  $X0$  and excited state  $B0$ .

A narrow range of pump laser wavelength for maximum population inversion in the ultraviolet domain is attributed to the near-resonance single-photon excitation accompanied by the Raman scattering. An anticorrelation between the population inversions corresponding to  $B0$ - $X0$  and  $B0$ - $X1$  transitions is related to the fact that level  $X1$  is populated from  $B0$  during the laser pulse.

By contrast, a broad peak around 1000 nm is strongly blue-shifted from the expected position at 1173 nm due to the three-photon ac Stark effect. The direct calculation of the population inversion using the density matrix formalism is qualitatively confirmed by the Floquet method. Similarly to the dc Stark effect, the energy gap between the ground and excited levels always increases from the free-field position for three-photon process. The three-photon transition dominates and leads to an efficient population transfer to  $B0$  level. A similar effect is expected in the wavelength domain of 1500–1800 nm due to the five-photon process. However, more simulations show that the probability of this process is much lower and no population inversion is expected. A similar process of population inversion should also occur for the oxygen atom.

#### ACKNOWLEDGMENTS

This work was supported by the National Natural Science Foundation of China (Grants No. 12204308, No. 12034013, and No. 12374318) and the Shanghai Science and Technology Commission (Grant No. 22ZR1444100).

#### APPENDIX A: RELEVANT MOLECULAR PARAMETERS

TABLE I. The vibration-dependent energy gap  $\Delta\mathcal{E}_{vv'}$  and transition dipole moment  $\mu_{vv'}$  between the  $N_2^+$  electronic states  $X^2\Sigma_g^+$  and  $A^2\Pi_u$ . The magnitude of dipole moments is calculated from the Einstein coefficients  $A_{ab}$  provided in Ref. [29], and the sign is calculated numerically by the diagonalization for three potential curves [24].

$N_2^+(v-v')$	$\Delta\mathcal{E}_{vv'}$ (a.u.)	$\mu_{vv'}$ (a.u.)
$X(0)-A(0)$	0.04145	0.1764
$X(0)-A(1)$	0.05006	0.1488
$X(0)-A(2)$	0.05854	0.0977
$X(0)-A(3)$	0.06687	0.0570
$X(0)-A(4)$	0.07507	0.0313
$X(1)-A(0)$	0.03145	-0.1505
$X(1)-A(1)$	0.04006	0.0466
$X(1)-A(2)$	0.04854	0.1241
$X(1)-A(3)$	0.05688	0.1182
$X(1)-A(4)$	0.06507	0.0862
$X(2)-A(0)$	0.02160	0.0808
$X(2)-A(1)$	0.03021	-0.1421
$X(2)-A(2)$	0.03869	-0.0350
$X(2)-A(3)$	0.04703	0.07446
$X(2)-A(4)$	0.05523	0.1107
$X(0)-B(0)$	0.11752	0.5783
$X(0)-B(1)$	0.12842	0.3596
$X(0)-B(2)$	0.13911	0.1258
$X(0)-B(3)$	0.14946	-0.0235
$X(0)-B(4)$	0.15959	0.0004
$X(1)-B(0)$	0.10754	0.3769
$X(1)-B(1)$	0.11843	-0.3412
$X(1)-B(2)$	0.12911	-0.4175
$X(1)-B(3)$	0.13949	0.1901
$X(1)-B(4)$	0.14956	0.1217
$X(2)-B(0)$	0.09769	0.2003
$X(2)-B(1)$	0.10858	-0.3985
$X(2)-B(2)$	0.11926	0.1627
$X(2)-B(3)$	0.12965	-0.4207
$X(2)-B(4)$	0.13974	-0.2352

## APPENDIX B: FLOQUET MATRIX

The Floquet matrix is calculated for  $X$  and  $B$  levels from the time-dependent Schrödinger equation, assuming a laser field of a constant amplitude and frequency  $\omega$ . It utilizes the time periodicity of the system Hamiltonian and considers

$$\begin{pmatrix} \cdot & \cdot & \cdot & \cdot & \cdot & \cdot & \cdot & \cdot & \cdot \\ \cdot & \mathcal{E}_B - 2\omega & \Omega/2 & 0 & 0 & 0 & 0 & 0 & \cdot \\ \cdot & \Omega^*/2 & \mathcal{E}_X - \omega & 0 & 0 & \Omega/2 & 0 & 0 & \cdot \\ \cdot & 0 & 0 & \mathcal{E}_B - \omega & \Omega^*/2 & 0 & 0 & 0 & \cdot \\ \cdot & 0 & 0 & \Omega^*/2 & \mathcal{E}_X & 0 & 0 & \Omega/2 & \cdot \\ \cdot & 0 & \Omega^*/2 & 0 & 0 & \mathcal{E}_B & \Omega/2 & 0 & \cdot \\ \cdot & 0 & 0 & 0 & 0 & \Omega^*/2 & \mathcal{E}_X + \omega & 0 & \cdot \\ \cdot & 0 & 0 & 0 & \Omega^*/2 & 0 & 0 & \mathcal{E}_B + \omega & \Omega/2 & \cdot \\ \cdot & 0 & 0 & 0 & 0 & 0 & 0 & \Omega^*/2 & \mathcal{E}_X + 2\omega & \cdot \\ \cdot & \cdot & \cdot & \cdot & \cdot & \cdot & \cdot & \cdot & \cdot \end{pmatrix}.$$

only the information in the frequency domain for  $X$  and  $B$  states.  $\mathcal{E}_{X/B}$  denotes the energy of the vibrational level in the electronic state  $X$  or  $B$ , and  $\Omega = -\mu_{XB}^{vv'} E_0 \cos \theta$  is the Rabi frequency. Transitions with up to five photons are considered.

The matrix of the Floquet Hamiltonian has the following form [28]:

- [1] A. Dogariu, J. B. Michael, M. O. Scully *et al.*, High-gain backward lasing in air, *Science* **331**, 442 (2011).
- [2] J. Yao, B. Zeng, H. Xu, G. Li, W. Chu, J. Ni, H. Zhang, S. L. Chin, Y. Cheng, and Z. Xu, High-brightness switch-able multiwavelength remote laser in air, *Phys. Rev. A* **84**, 051802(R) (2011).
- [3] P. R. Hemmer, R. B. Miles, P. Polynkin, T. Siebert, A. V. Sokolov, P. Sprangle, and M. O. Scully, Standoff spectroscopy via remote generation of a backward-propagating laser beam, *Proc. Natl. Acad. Sci. USA* **108**, 3130 (2011).
- [4] X. Zhang, Q. Lu, H. C. Mei, S. Y. Qin, Y. Gao, A. Houard, V. T. Tikhonchuk, A. Mysyrowicz, L. Xu, and Y. Liu, Standoff detection of an electric field by bidirectional nitrogen lasing, *Phys. Rev. A* **108**, 033513 (2023).
- [5] J. Ni, W. Chu, H. Zhang, B. Zeng, J. Yao, L. Qiao, G. Li, C. Jing, H. Xie, H. Xu, Y. Cheng, and Z. Xu, Impulsive rotational Raman scattering of  $N_2$  by a remote “air laser” in femtosecond laser filamen, *Opt. Lett.* **39**, 2250 (2014).
- [6] Z. Zhang, F. Zhang, B. Xu, H. Xie, B. Fu, X. Lu, N. Zhang, S. Yu, J. Yao, Y. Cheng, and Z. Xu, High-sensitivity gas detection with air-lasing-assisted coherent raman spectroscopy, *Ultrafast Sci.* **2022**, 9761458 (2022).
- [7] H. Lei, J. Yao, J. Zhao, H. Xie, F. Zhang, H. Zhang, N. Zhang, G. Li, Q. Zhang, X. Wang, Y. Yang, L. Yuan, Y. Cheng, and Z. Zhao, Ultraviolet supercontinuum generation driven by ionic coherence in a strong laser field, *Nat. Commun.* **13**, 4080 (2022).
- [8] Y. Wan, Z. Liu, J. Yao, B. Xu, J. Chen, F. Zhang, Z. Zhang, L. Qiao, and Y. Cheng, A spectrally bright wavelength-switchable vacuum ultraviolet source driven by quantum coherence in strong-field-ionized molecules, *New J. Phys.* **23**, 023005 (2021).
- [9] L. Yuan, Y. Liu, J. Yao, and Y. Cheng, Recent advances in air lasing: A perspective from quantum coherence, *Adv. Quantum Technol.* **2**, 1900080 (2019).
- [10] H. Xu, E. Lötstedt, A. Iwasaki, and K. Yamanouchi, Sub-10-fs population inversion in  $N_2^+$  in air lasing through multiple state coupling, *Nat. Commun.* **6**, 8347 (2015).
- [11] J. Yao, S. Jiang, W. Chu, B. Zeng, C. Wu, R. Lu, Z. Li, H. Xie, G. Li, C. Yu, Z. Wang, H. Jiang, Q. Gong, and Y. Cheng, Population redistribution among multiple electronic states of molecular nitrogen ions in strong laser fields, *Phys. Rev. Lett.* **116**, 143007 (2016).
- [12] Q. Zhang, H. Xie, G. Li, X. Wang, H. Lei, J. Zhao, Z. Chen, J. Yao, Y. Cheng, and Z. Zhao, Sub-cycle coherent control of ionic dynamics via transient ionization injection, *Commun. Phys.* **3**, 50 (2020).
- [13] A. Mysyrowicz, R. Danylo, A. Houard, V. Tikhonchuk, X. Zhang, Z. Fan, Q. Liang, S. Zhuang, L. Yuan, and Y. Liu, Lasing without population inversion in  $N_2^+$ , *APL Photonics* **4**, 110807 (2019).
- [14] V. T. Tikhonchuk, Y. Liu, R. Danylo, A. Houard, and A. Mysyrowicz, Theory of femtosecond strong field ion excitation and subsequent lasing in  $N_2^+$ , *New J. Phys.* **23**, 023035 (2021).
- [15] C. Kleine, M.-O. Winghart, Z.-Y. Zhang, M. Richter, M. Ekimova, S. Eckert, M. J. J. Vrakking, E. T. J. Nibbering, A. Rouzée, and E. R. Grant, Electronic state population dynamics upon ultrafast strong field ionization and fragmentation of molecular nitrogen, *Phys. Rev. Lett.* **129**, 123002 (2022).
- [16] R. Danylo, G. Lambert, M. Redkin, A. Houard, X. Zhang, Y. Liu, L. Xu, A. Couairon, V. Tikhonchuk, and A. Mysyrowicz, Evolution of the populations of ionic electronic levels during lasing of molecular nitrogen at 391.4 nm: Evidence of a two photon amplification process in a V scheme arrangement (unpublished).
- [17] M. Richter, M. Lytova, F. Morales, S. Haessler, O. Smirnova, M. Spanner, and M. Ivanov, Rotational quantum beat lasing without inversion, *Optica* **7**, 586 (2020).
- [18] H. Li, M. Hou, H. Zang, Y. Fu, E. Lötstedt, T. Ando, A. Iwasaki, K. Yamanouchi, and H. Xu, Significant enhancement of  $N_2^+$  lasing by polarization-modulated ultrashort laser pulse, *Phys. Rev. Lett.* **122**, 013202 (2019).
- [19] H. Li, E. Lötstedt, H. Li, Y. Zhou, N. Dong, L. Deng, P. Lu, T. Ando, A. Iwasaki, Y. Fu, S. Wang, J. Wu, K. Yamanouchi, and H. Xu, Giant enhancement of air lasing by complete

- population inversion in  $N_2^+$ , *Phys. Rev. Lett.* **125**, 053201 (2020).
- [20] M. O. Scully and M. S. Zubairy, *Quantum Optics* (Cambridge University Press, Cambridge, England, 1997).
- [21] J. Chen, J. Yao, H. Zhang, Z. Liu, B. Xu, W. Chu, L. Qiao, Z. Wang, J. Fatome, O. Faucher, C. Wu, and Y. Cheng, Electronic-coherence-mediated molecular nitrogen-ion lasing in a strong laser field, *Phys. Rev. A* **100**, 031402(R) (2019).
- [22] X. M. Tong, Z. X. Zhao, and C. D. Lin, Theory of molecular tunneling ionization, *Phys. Rev. A* **66**, 033402 (2002).
- [23] S.-F. Zhao, C. Jin, T. F. Jiang, and C. D. Lin, Determination of structure parameters in strong-field tunneling ionization theory of molecules, *Phys. Rev. A* **81**, 033423 (2010).
- [24] L. Xu, Q. Lu, V. T. Tikhonchuk, B. Zhou, R. Yang, Q. Liang, F. He, R. Danylo, A. Houard, A. Mysyrowicz, and Y. Liu, Quantum and quasi-classical effects in the strong field ionization and subsequent excitation of nitrogen molecules, *Opt. Express* **30**, 38481 (2022).
- [25] V. T. Tikhonchuk, Y. Liu, R. Danylo, A. Houard, and A. Mysyrowicz, Modeling of the processes of ionization and excitation of nitrogen molecules by short and intense laser pulses, *Phys. Rev. A* **104**, 063116 (2021).
- [26] S. Wang, E. Lotstedt, J. Cao, Y. Fu, H. Zang, H. Li, T. Ando, A. Iwasaki, K. Yamanouchi, and H. Xu, Population inversion in  $N_2^+$  by vibrationally mediated Rabi oscillation at 400 nm, *Phys. Rev. A* **104**, L010201 (2021).
- [27] Q. Lu, X. Zhang, S. López, H. Mei, L. Xu, Q. Liang, A. Houard, V. Tikhonchuk, A. Mysyrowicz, E. Oliva, and Y. Liu, Spectral splitting of the lasing emission of nitrogen ions pumped by 800-nm femtosecond laser pulses, *Opt. Lett.* **48**, 664 (2023).
- [28] R. V. Krems, *Molecules in Electromagnetic Fields* (John Wiley & Sons, New York, 2019).
- [29] F. R. Gilmore, R. R. Laher, and P. J. Espy, Franck-Condon factors, r-Centroids, electronic transition moments, and Einstein coefficients for many nitrogen and oxygen band system, *J. Phys. Chem. Ref. Data* **21**, 1005 (1992).